Biomaterials Science

ROYAL SOCIETY OF CHEMISTRY

PAPER

View Article Online
View Journal | View Issue

Cite this: *Biomater. Sci.*, 2023, **11**, 533

An antibacterial and proangiogenic double-layer drug-loaded microneedle patch for accelerating diabetic wound healing

Shan Gao,†[a] Wanlin Zhang,†[a] Xingxing Zhai,[a] Xue Zhao,[a] Jianxin Wang,[b] Jie Weng,*[a,b] Jianshu Li[c] and Xingyu Chen*[a]

Received 30th September 2022,
Accepted 13th November 2022

DOI: 10.1039/d2bm01588a

rsc.li/biomaterials-science

Diabetic wounds are difficult to heal because of bacterial infections and insufficient angiogenesis. Herein, we report a double-layer drug-loaded microneedle patch with antibacterial and angiogenesis-promoting properties for diabetic wound healing. The double-layer microneedle comprises the hyaluronic acid (HA)-loaded antibacterial drug tetracycline hydrochloride (TCH) as the tip and a mixture of chitosan and silk fibroin containing the angiogenic drug deferoxamine (DFO) as the substrate. In the double-layer drug-loaded microneedle system (DMN@TCH/DFO), rapid dissolution of HA at the tip releases TCH to promote early antibacterial activity. The substrate exhibits excellent swelling properties, facilitating the absorption of tissue fluid from the wound to promote wound contraction. Simultaneously, DFO is released to promote angiogenesis. Therefore, DMN@TCH/DFO exhibited adequate mechanical properties, excellent swelling and biocompatibility, antibacterial properties, and angiogenesis-promoting capabilities. In a wound model of diabetic rats, DMN@TCH/DFO reduced inflammatory responses, promoted angiogenesis, and facilitated collagen deposition, thereby accelerating diabetic wound healing. Overall, DMN@TCH/DFO can accelerate the healing of diabetic wounds and has clinical application prospects.

1. Introduction

Diabetic foot ulcers are a common and serious complication of diabetes, with approximately 15–25% of patients with diabetes experiencing diabetic foot ulcer complications.[1] If left untreated, most foot ulcers lead to skin ulceration and tissue necrosis, and even lower limb amputation, which considerably increases the risk of death of patients.[2] Acute wounds trigger a wound-healing response that comprises four distinct and overlapping phases: hemostasis, inflammation, proliferation, and remodeling. Unfortunately, these processes are impaired in diabetes-induced chronic wounds.[3,4] The primary reason for the difficulty in healing chronic diabetic wounds is the presence of biofilms, which are produced by bacteria colonizing the wound area, predominantly *Staphylococcus aureus*.[5] Bacteria in biofilms are multidrug-resistant, and biofilms act as physical barriers, preventing the penetration of antibiotics or other therapeutic drugs.[6] Another important factor attributed to the difficulty in the healing of chronic diabetic wounds is poor angiogenesis, resulting in insufficient vascular perfusion, which prevents the delivery of sufficient nutrients, oxygen, and other necessities for wound healing.[7]

The treatment of chronic diabetic wounds has been extensively explored, and the current traditional treatment options are wound debridement, off-loading, and the use of antibiotics to control infection.[8–10] These methods have some disadvantages, including the pain caused by frequent surgical debridement,[11] complex devices and procedures of off-loading therapy that may lead to poor patient compliance,[12] and the side effects of resistance to systemic antibiotics.[13] Therefore, many wound dressings, including films, hydrocolloids, and hydrogels, have been developed, most of which have limitations owing to their biofilm impermeability.[14]

Microneedles (MNs) are needles with a height of 10–2000 μm and are widely used in transdermal drug delivery systems (TDDSs).[15] MNs have many advantages over conventional wound dressings in treating diabetic wounds because they can destroy biofilms and deliver drugs at a deeper level.[16,17] For instance, Xu *et al.* studied the use of MNs for bacterial biofilm treatment. After applying the MN patch, the

[a]*College of Medicine, Southwest Jiaotong University, Chengdu 610031, China. E-mail: jweng@swjtu.edu.cn, chenxy@swjtu.edu.cn*
[b]*Key Laboratory of Advanced Technologies of Materials (Ministry of Education), School of Materials Science and Engineering, Southwest Jiaotong University, Chengdu 610031, China*
[c]*College of Polymer Science and Engineering, Sichuan University, Chengdu 610065, China*
†These authors equally contributed to this work and should be considered as co-first authors.

integrity of the biofilm was destroyed, and the dyes loaded on the MN patch diffused efficiently into the biofilm matrix.[18] In recent years, the use of MNs in wound healing has been widely studied.[19,20] Woodhouse *et al.* proposed a highly water-soluble MN patch loaded with calcium peroxide (CPO), which degrades into hydrogen peroxide and oxygen upon exposure to water, killing bacteria in wounds and oxygenating local tissue to promote wound healing.[19] Chi *et al.* developed a novel Chinese herbal MN patch based on two Chinese herbs, *Premna microphylla* and *Centella asiatica*, with outstanding antibacterial activity in inflammation inhibition, angiogenesis, collagen deposition, and tissue reconstruction.[20] MNs are also an effective platform for the delivery of many smart and responsive therapeutics. Sun *et al.* loaded metal–organic framework-derived peroxidase-like nanozymes in MN patches, which converted light energy into heat energy to enhance drug permeability while decomposing hydrogen peroxide into hydroxyl radicals for antibacterial use on wounds.[21] Thus, wound therapeutic methods combined with emerging microneedle drug delivery systems can produce excellent results.

Herein, we report an antibacterial and angiogenesis-promoting double-layer drug-loaded microneedle (DMN@TCH/DFO) for accelerated diabetic wound healing (Scheme 1). Sodium hyaluronate (HA), a biocompatible polysaccharide,[22] was used to prepare dissolvable tips of MNs.[23] Chitosan (CS) exhibits excellent biocompatibility, hemostasis, antibacterial, bioadhesive, and biodegradable properties.[24] However, the use of CS as a wound dressing material is limited owing to its poor mechanical properties.[25] Silk fibroin (SF) exhibits good mechanical properties and excellent toughness and ductility.[26,27] Therefore, SF and CS composites can enhance the mechanical properties and toughness of the backing. The antimicrobial agent tetracycline hydrochloride (TCH) and the angiogenic drug deferoxamine (DFO) were loaded into the tip and the substrate of the double-layer MN, respectively. When the MN patch was applied to a wound, the MN tip destroyed the biofilm, and HA at the needle tip rapidly dissolved to release TCH for its antibacterial activity. The substrate absorbed tissue fluid at the wound and swelled, which facilitated the slow release of DFO and its deep delivery along the hole left by the needle tip for angiogenesis. In *in vivo* experiments, DMN@TCH/DFO showed excellent antibacterial and angiogenic activities, significantly enhancing tissue regeneration and wound healing. Overall, our DMN system possesses remarkable potential for clinical applications in diabetic wound healing.

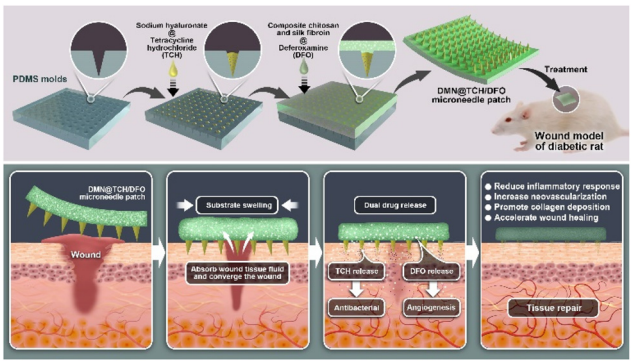

Scheme 1 Schematic of the fabrication of the double-layer drug-loaded microneedle and its accelerated healing of diabetic wounds by resisting bacteria, reducing inflammation, and promoting angiogenesis and collagen regeneration.

2. Materials and methods

2.1. Materials

Chitosan (CS; deacetylation degree ≥95%) and deferoxamine mesylate (DFO) were purchased from Shanghai Aladdin Biochemical Technology Co., Ltd (Shanghai, China). Natural silkworm cocoons were purchased from Jiuheng Silk Products Management Department, Nanxun Lian City. Sodium hyaluronate (HA; MW 200 kDa–400 kDa) was purchased from Bloomage Freda Biopharm Co., Ltd (Shandong, China). Polydimethylsiloxane (PDMS) molds were purchased from Taizhou Microchip Pharmaceutical Technology Co., Ltd (Taizhou, China). Tetracycline hydrochloride (TCH) was obtained from Shanghai Macklin Biochemical Co., Ltd (Shanghai, China). A Cell Counting Kit-8 (CCK-8) was obtained from Dojindo Laboratories (Kumamoto, Japan). Dulbecco's modified Eagle's medium (DMEM), fetal bovine serum (FBS), and a 1% penicillin–streptomycin solution were purchased from HyClone Laboratories (Logan, UT, USA). L929 cells were purchased from Tianjin Ruiboxing Biotechnology Co., Ltd (Tianjin, China). Human umbilical vein endothelial cells (HUVECs) were obtained from the National Collection of Authenticated Cell Cultures (Shanghai, China). Male Sprague–Dawley rats were purchased from Chengdu Dossy Experimental Animals Co., Ltd (Chengdu, China). All reagents were used as received without further purification. All the solutions were prepared using deionized water.

2.2. Preparation of SF solution

The silkworm cocoons were boiled in a 0.02 M Na_2CO_3 solution at 100 °C for 60 min, removed, and rinsed with deionized water three times to completely remove sericin (glue protein). Silk fibroins were dried at 60 °C overnight and then dissolved in a 9.3 M LiBr solution at 60 °C under stirring at a constant temperature for 4 h to obtain a brownish yellow solution. The solubilized silk fibroin solution was dialyzed against deionized water for 3 d to remove small molecules. The dialysis bag was then placed into a polyethylene glycol solution for 16 h for reverse dialysis. After reverse dialysis, the silk fibroin solution was centrifuged at 10 000 rpm for 20 min to remove undissolved silk fibroin fibers. After quantification, the silk fibroin was diluted to 7.0% and stored at 4 °C.

2.3. Preparation of double-layer microneedle patches

PDMS molds were used to create microneedle patches. A 10 wt% HA solution was prepared by dissolving the HA powder

in deionized water. The CS powder was dissolved in a 2% acetic acid solution by heating and stirring to obtain a 4 wt% CS solution. The CS and SF solutions were mixed in a ratio of 4 : 1 under constant stirring, and then a 1 wt% genipin solution was added to obtain the microneedle substrate material. First, to prepare the microneedle tip, the PDMS mold was filled with the HA solution, centrifuged at 3000 rpm and 25 °C for 5 min, and then dried for 30 min. After that, the PDMS mold was filled with the CS and SF solutions to prepare the microneedle substrate. The microneedle substrate was dried overnight and demolded to obtain a blank double-layer microneedle patch (blank DMN). For DMN@TCH patches, different concentrations of TCH (1, 2, and 3 mg mL^{-1}) were dissolved in the HA solution as microneedle tips, according to the preparation of the blank DMN. The DMN@TCH patches were designated as DMN@TCH-1, DMN@TCH-2, and DMN@TCH-3, respectively. Similarly, for DMN@DFO patches, different concentrations of DFO (0.1, 0.5, 1, and 2 mg mL^{-1}) were dissolved in the mixture solution of CS and SF as microneedle substrates and labeled as DMN@DFO-0.1, DMN@DFO-0.5, DMN@DFO-1, and DMN@DFO-2, respectively. For DMN@TCH/DFO, the concentration of TCH was 2 mg mL^{-1} at the tip, and the concentration of DFO was 0.1 mg mL^{-1} in the substrate.

2.4. Mechanical properties test

The mechanical properties of the blank DMN were measured using a universal testing machine. The microneedle patch was fixed on the universal testing machine with the tips facing upward, with the breaking strength of the needle tip was measured at a test speed of 5 mm min^{-1}.

A skin insertion test was performed on *ex vivo* porcine skin. Full-thickness pig carcass skin was cut into small pieces, and the skin was stretched and fixed on a flat surface. Blank DMN was pierced into the pig carcass skin and removed from the skin after 2 min. Pictures of the treated areas were taken and observed. Furthermore, skin recovery after blank DMN insertion was evaluated *in vivo* using shaved rat dorsal skin. The blank DMN was inserted into the dorsal skin of the rats for 2 min and then removed. Blank DMN application areas were photographed at 0, 3, and 10 min after insertion.

2.5. Dissolution and swelling properties

Agar was pierced with the blank DMN, which was pulled off after 5 min and the changes in the microneedle tips were recorded by photography. The blank DMN was weighed and placed in a phosphate-buffered saline (PBS, pH 7.4) solution. After 24 h, the blank DMN was removed, the surface water was removed using filter paper, and the DMN was weighed again. The swelling ratio of the blank DMN was calculated using the following formula:

$$\text{Swelling Ratio } (\%) = (W_1 - W_0)/W_0 \times 100\%$$

where W_1 and W_0 represent the swollen and initial weights of the blank DMN, respectively.

2.6. *In vitro* antibacterial activity

The antibacterial activity of DMN@TCH against *Staphylococcus aureus* (*S. aureus*) and *Escherichia coli* (*E. coli*) was investigated. The blank DMN and DMN@TCH patches (DMN@TCH-1, DMN@TCH-2, and DMN@TCH-3) were cut into pieces (5 × 5 needle tips). *S. aureus* and *E. coli* incubated overnight were diluted to 10^6 CFU mL^{-1} in a Langmuir–Blodgett (LB) medium. The bacterial suspension (100 μL) was plated onto an agar plate. The blank DMN and DMN@TCH pieces were then placed onto the bacteria-coated agar plate with the tips inside the agar. After incubation at 37 °C for 24 h, the diameters of the inhibition zones were measured and photographed. Three parallel samples were used for each treatment group. The blank DMN and DMN@TCH pieces were also co-cultured with the bacterial suspension for 12 h. The bacterial solution was then diluted 1000 times and coated on an agar plate, and the colonies on the plate were photographed after culturing in the incubator. The group without DMN was used as the control group.

2.7. Cell experiments

2.7.1. Cytocompatibility evaluation. L929 cells were used to study the cytotoxicity of the blank DMN. L929 cells were seeded in a 96-well plate at a density of 5000 cells per well and were incubated with hydrogels at 37 °C under an atmosphere of 5% CO_2 for 24 h. The blank DMN was cut into small pieces and incubated with L929 cells (the concentration of the blank DMN was 10 mg mL^{-1}). Cell viability was determined using CCK-8 after 1 and 3 d of incubation. CCK-8 solution (10 μL) and cell culture medium (100 μL) were added to each well. After incubating the plate in a cell incubator for 2 h, the solution was transferred to a 96-well plate. The absorbance of the solution was measured using a microplate reader (UV3600; Shimadzu, Japan) at a wavelength of 450 nm.

2.7.2. Cell proliferation. HUVECs were used to study the effect of the DMN@DFO patches (DMN@DFO-0.1, DMN@DFO-0.5, DMN@DFO-1, and DMN@DFO-2) on cell proliferation. HUVECs were seeded in a 96-well plate at a density of 3000 cells per well. The DMN@DFO patches were sterilized with UV light and then incubated with HUVECs. Cell viability was determined using the CCK-8 assay after 1, 2, and 3 d of incubation.

2.7.3. HUVEC tube-formation assay. The *in vitro* vascularization capacity of DMN@DFO was assessed using tube formation assays. Matrigel (10 mg mL^{-1}) was placed onto 48-well plates for HUVEC culture, and DMN@DFO-0.1 and DMN@DFO-0.5 extracts (10 mg mL^{-1}) were added. After incubation for 12 h, tube formation was observed under a microscope and photographed. The average length of a tube was determined using ImageJ software.

2.8. Drug release *in vitro*

DMN@TCH was immersed in 5 mL of PBS (pH 7.4) solution and, at different time intervals, 500 μL of buffer was removed

and another 500 μL of fresh buffer was added. The extracted solution was analyzed by measuring its absorbance at a wavelength of 360 nm using a microplate reader. Similarly, DMN@DFO was placed in deionized water, and at predetermined times, 500 μL of buffer was removed and another 500 μL of deionized water was added. The extracted solution was centrifuged and mixed with an $FeCl_3$ solution (6 mM) in equal proportions. DFO released from the backing was analyzed by measuring the absorbance of the solution at a wavelength of 485 nm using a microplate reader. Three samples were tested in the experiment to ensure reproducibility, and the average data were then calculated.

2.9. *In vivo* wound healing

Animal experiments were performed using 8-week-old male Sprague–Dawley rats (210–250 g). The animal experiments were conducted in accordance with the protocols adopted by the Medical Ethics Committee of Southwest Jiaotong University (SWJTU-2013-023) and the guidelines of the laboratory animal administration rules of China. To induce type I diabetes, the rats were fasted for 12 h and then injected intraperitoneally with streptozotocin (STZ, 60 mg kg^{-1}). Five days after STZ injection, the blood glucose level of the rats was measured in the tail vein, and the rats with plasma glucose ≥16.7 mM were considered to have type I diabetes.

Diabetic rats were randomly divided into three groups, with five rats in each group. Rats were anesthetized with 10% chloral hydrate (3.5 mL kg^{-1}) prior to surgery. After shaving and sterilization, three full-thickness wounds with a diameter of 10 mm were made on the back of each rat. The wounds were treated with normal saline, blank DMN, and DMN@TCH/DFO. The patch was secured with a medical applicator and bandage to prevent it from falling off. The wound areas were photographed on days 0, 3, 7, and 14. The area of each wound was measured using ImageJ.

On days 3, 7, and 14, four rats were sacrificed, and wound samples were taken, fixed with 4% paraformaldehyde, and paraffin-embedded. Hematoxylin and eosin (H&E) and Masson's trichrome staining were used to analyze histological changes and collagen deposition at different stages of healing. On days 3 and 7, immunohistochemical staining for CD31 and TNF-α was performed to assess wound vascularization and inflammatory responses. Immunohistochemical staining was also performed on collagen type I and type III at different times to assess wound collagen deposition. The images of stained sections were captured using a light microscope.

2.10. Statistical analysis

The data were expressed as mean ± standard deviation (SD) and analyzed using one-way analysis of variance (ANOVA) to compare treatment and control groups. $^{*}P < 0.05$ and $^{**}P < 0.01$ were considered significant.

3. Results and discussion

3.1. Characterization of microneedles

Here, we fabricated double-layer microneedle patches. Fig. 1a shows that the topography of the blank DMN obtained by demolding was a neatly arranged array of 10 × 10 microneedles. Fig. 1b shows the SEM image of the blank DMN. The needle tips of the blank DMN are pyramidal, complete, uniform, and sharp with a height of approximately 1000 μm.

Fig. 1c shows the force–displacement curve, where the maximum failure force of the entire microneedle array (10 × 10) was 162 N. Therefore, the maximum failure force of the blank DMN was calculated to be 1.62 N per needle, which was significantly greater than the minimum force required to pierce skin (0.1 N).[28,29] Furthermore, the isolated pig skin and the back skin of an SD rat were used to test the effect of the blank DMN puncture. The blank DMN was applied to the pig skin for 2 min and then removed. In Fig. 1d, well-arranged microporous channels in the skin can be observed, indicating that the blank DMN was strong and sharp enough to penetrate the skin. Fig. 1e shows the insertion of the blank DMN into the back skin of a living SD rat; no other side effects were observed except for the microholes formed by the needle tips and pan-infrared coloring at the insertion site. The microchannels generated by the blank DMN were almost resealed in 10 min. Rapid closure of the microchannels reduces the risk of pathogenic microbial invasion, indicating the good recovery

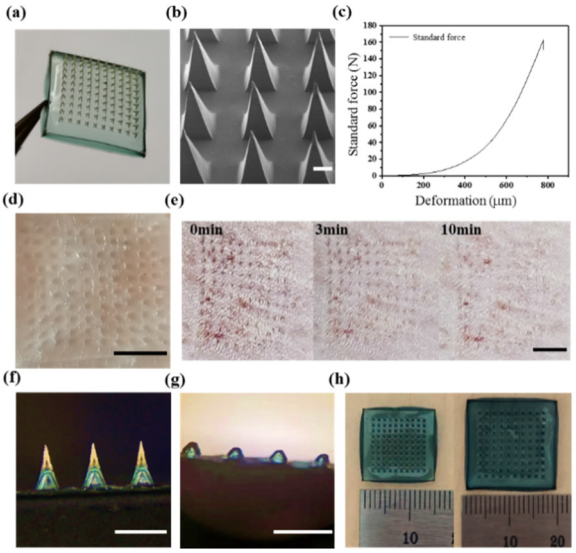

Fig. 1 Characterization of the double-layer microneedle patch. (a) Camera image of the blank DMN; (b) SEM image of the blank DMN (scale bar: 300 μm); (c) mechanical properties characterization of the blank DMN; (d) photograph of the pores left after DMN was applied to the isolated pig skin (scale bar: 500 mm); (e) images of the rat back skin treated with the blank DMN (scale bar: 500 mm); (f) blank DMN photographed using a light microscope (scale bar: 1000 μm); (g) photograph of the blank DMN inserted into agar for 5 minutes and then removed (scale bar: 1000 μm); (h) photograph of the blank DMN before (left) and after (right) swelling.

ability of the skin after microneedle insertion, which may improve patient compliance.[22]

Because the tip and the substrate of the double-layer microneedle patches are made of different materials, the binding of the interface and the solubility of the DMN were investigated. The image of the blank DMN in Fig. 1f indicates delamination between the tip and backing while remaining well connected to each other. Most of the tips were dissolved after the blank DMN was inserted into the agar (Fig. 1g), indicating that the HA on the tips could be rapidly dissolved. Compared with insoluble tips, the dissolved tips do not remain in the body, making them more suitable for wound applications. Fig. 1h shows that the volume of the blank DMN substrate increases significantly because of its swelling, with a swelling ratio of 324 ± 15%. The ability of the blank DMN substrate to absorb moisture helps accelerate the wound healing process by absorbing wound exudate and reducing the probability of infection.

3.2. *In vitro* antibacterial activity

Microneedle-tip drug loading can deliver drugs to the depth of the wound and achieve a better therapeutic effect. Agar plate diffusion tests were performed on the blank DMN and DMN@TCH patches to evaluate their bactericidal activity. Regardless of the presence of *S. aureus* or *E. coli*, the zones of inhibition were observed around all the DMN@TCH samples but not around the blank DMN sample (Fig. 2a). The diameter of the inhibition zone of each sample was calculated using ImageJ. For DMN@TCH-1, *E. coli* and *S. aureus* agar plates produced inhibition zones with a diameter of 13.1 ± 90.11 and 21.89 ± 1.44 mm, respectively (Fig. 2b). For DMN@TCH-2, *E. coli* and *S. aureus* agar plates produced inhibition zones with a diameter of 20.81 ± 1.20 and 27.48 ± 1.03 mm, respectively. Significant differences were observed in the sizes of the inhibition zones of DMN@TCH-2 and DMN@TCH-1; however, DMN@TCH-3 and DMN@TCH-2 displayed no significant difference. Therefore, DMN@TCH-2 exhibited a good antibacterial effect and required a lower dosage of the antibacterial agent.

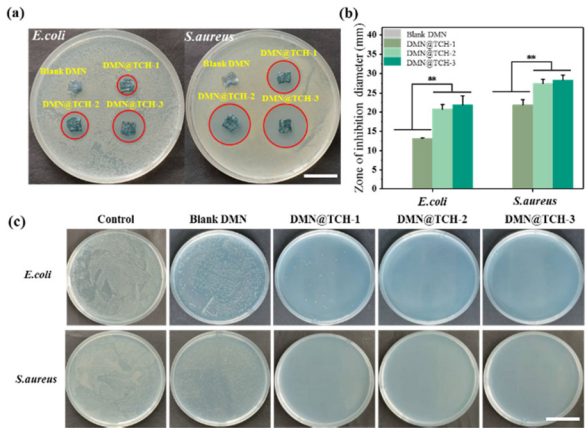

Fig. 2 *In vitro* antibacterial activity of DMN@TCH patches. (a) Inhibition zone study of microneedle patches against *E. coli* and *S. aureus* (the red circle represents the inhibition zone, scale bar: 20 mm); (b) the size of inhibition zone (mean ± SD, $n = 3$), $^{**}p < 0.01$; (c) bacterial colonization images of *S. aureus* and *E. coli* on agar plates after treating with the DMN@TCH patches, scale bar: 30 mm.

The antibacterial activity of DMN@TCH was also evaluated by co-culturing it with bacteria. Compared with the control group, the blank DMN inhibited the growth of bacteria to some extent (Fig. 2c). In the inhibition zone experiment, the bactericidal effect of the microneedle patch was due only to drug release from the tips. However, in the co-cultivation experiment, the swelling of the DMN substrate reduced the bacterial concentration. In addition, compared to the blank DMN, the antibacterial ability of the DMN@TCH samples was significantly improved. Only a few bacterial colonies were found on the agar plate in the DMN@TCH-1 sample after co-culturing with *E. coli*, whereas no bacterial colonies were observed in the DMN@TCH-2 and DMN@TCH-3 samples. Moreover, no bacterial colonies were observed in any of the DMN@TCH samples after co-culturing with *S. aureus.* These results indicate that the antibacterial effect of DMN@TCH against *S. aureus* is better than that against *E. coli*, probably because the outer membrane of Gram-negative bacteria renders them more resistant to bactericides and bacteriostatic agents.[30] Therefore, the most effective concentration of TCH was 2 mg mL^{-1} because DMN@TCH-2 exhibited an excellent bactericidal effect and the lowest concentration of antibacterial agent.

3.3. *In vitro* cell activity

L929 cells and HUVECs were used to study the cell activity of the double-layer microneedle patches. Fig. 3a shows that the blank DMN exhibited no cytotoxicity and could be used as a biomaterial *in vivo*. The CCK-8 assay was used to evaluate the effect of DMN substrate loading with different DFO concentrations on HUVEC proliferation. As shown in Fig. 3b, DMN@DFO-0.1 promoted HUVEC proliferation. However, an increase in the DFO concentration in DMN resulted in its high toxicity, which further inhibited HUVEC growth. The fluorescence images of HUVECs also indicate that DMN@DFO-0.1 displayed the best growth state, with the highest cell density compared with the other samples (Fig. 3c). These results were consistent with the determination of cell viability using CCK-8.

Angiogenesis in the wound area is essential for its healing. DFO stimulates angiogenesis by upregulating VEGF and SDF-1α through the accumulation of HIF-1α.[31] DFO has been shown to enhance neovascularization through the accumulation of HIF-1α and the regulation of endothelial cell function.[32,33] Several studies have reported that DFO-loaded dressings have induced angiogenesis locally in wounds.[34–36] In this study, different concentrations of DFO were loaded onto the DMN substrate, and the tube formation assay was used to assess vascularization capacity. Compared with the control group, HUVECs treated with the blank DMN showed a certain effect in promoting angiogenesis (Fig. 3d), which may be attributed to the remarkable biocompatibility of the DMN components. In addition, DMN@DFO-0.1 showed the most

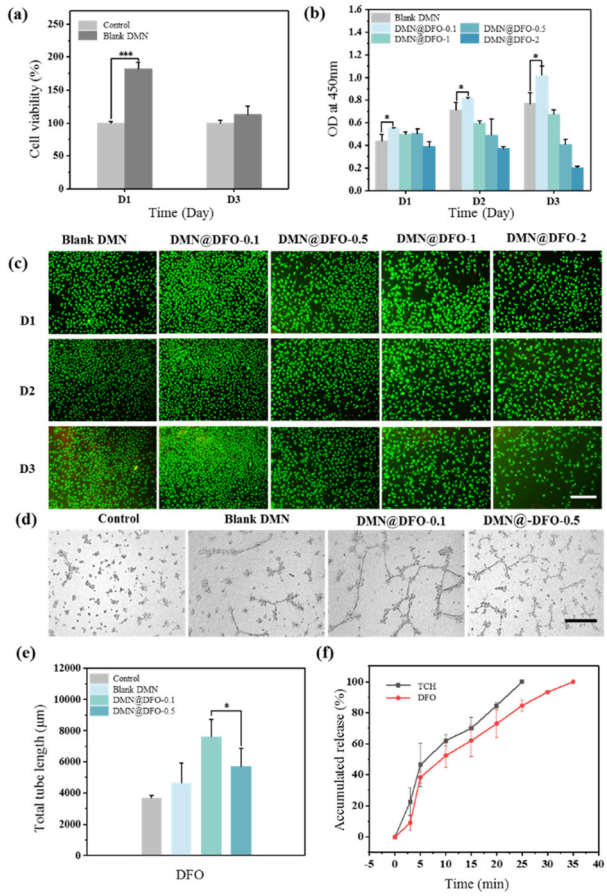

Fig. 3 *In vitro* cell biology studies and drug release studies. (a) Assessment of cytotoxicity of the blank DMN with L929 cells (mean ± SD, n = 3), ***p < 0.001; (b) cell proliferation measurements of HUVECs cultured with the DMN@DFO on days 1, 2, and 3 (mean ± SD, n = 3) *p < 0.05; (c) live and dead staining assay of HUVECs cultured with DMN@DFO on days 1, 2, and 3 (scale bar: 200 μm); (d) tube formation images photographed using a light microscope after HUVECs were incubated with the extract of DMN@DFO for 12 h (scale bar: 200 μm); (e) length quantification of the tubule network using ImageJ software (mean ± SD, n = 3), *p < 0.05; (f) *in vitro* release profiles of TCH and DFO.

comprehensive vascular tubule formation and the longest tube length among all samples (Fig. 3e), which was attributed to low-dose DFO release. This suggests that the DMN substrate with a low concentration of DFO exhibits an angiogenesis inducing effect, whereas its high concentration produces an inhibitory effect. A well-established vascular network can effectively promote the delivery of nutrients, thereby enhancing wound repair. Combined with the results of HUVEC proliferation and *in vitro* tube formation experiments, DMN@DFO-0.1 showed the best angiogenic activity and was used for subsequent *in vivo* experiments.

3.4. *In vitro* drug release

In the antibacterial and cell activity experiments, it was found that the best drug loading method for a double-layer drug-loaded microneedle was that loaded with 2 mg mL^{-1} of TCH in the tip and 0.1 mg mL^{-1} of DFO in the substrate, which was defined as DMN@TCH/DFO for subsequent experimental studies. Fig. 3f shows the release behavior of TCH and DFO; TCH was completely released in 25 min because HA at the DMN tip rapidly dissolved and released TCH. Compared with TCH release, the release behavior of DFO was relatively slower because it was released by adsorption and swelling of the DMN substrate. However, when DMN@TCH/DFO was applied to a wound *in vivo*, the swelling and drug release rates were slower owing to less fluid in the wound. Overall, DMN@TCH/DFO could release drugs in a programmed manner, quickly releasing TCH to achieve antimicrobial effects and gradually releasing DFO to promote angiogenesis.

3.5. *In vivo* wound healing in diabetic skin

The wound-healing ability of DMN@TCH/DFO *in vivo* was studied in a diabetic rat skin wound model (Fig. 4a). Representative images of wound contraction with each treatment sample were recorded to evaluate the wound healing process and quantitatively analyze the wound area using ImageJ software. As shown in Fig. 4b–d, the wounds in the control sample did not change significantly on the 3rd day,

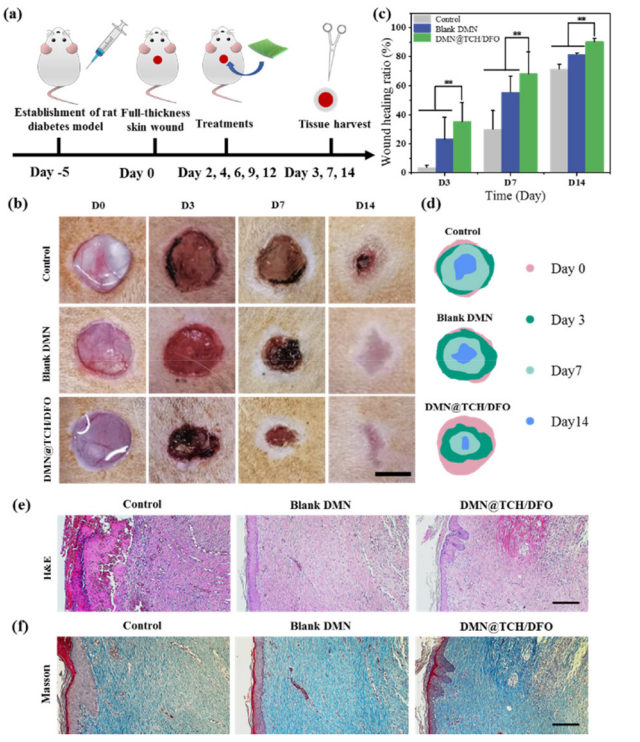

Fig. 4 *In vivo* evaluation of the double-layer drug-loaded microneedle accelerating diabetic wound healing. (a) Experimental timeline for the wound repair study; (b) wound images collected on days 0, 7, and 14 after treatment (scale bar: 5 mm); (c) wound healing ratio on days 3, 7, and 14 after treatment (mean ± SD, n = 3), **p < 0.01; (d) comparison of wound areas treated with various samples at various times; (e) H&E staining of wounds at day 14 (scale bar: 100 μm); (f) Masson staining of wounds at day 14 (scale bar: 100 μm).

while the wound area treated with the blank DMN and DMN@TCH/DFO was significantly reduced. This is because the swelling of the microneedle substrate can absorb tissue fluid at the wound site, causing the wound surface to dry and shrink. On day 7, about 68.13 ± 15.25% of wounds treated with DMN@TCH/DFO were closed, which was significantly higher than those treated with the blank DMN (55.44 ± 11.26%) and the control sample (30.04 ± 12.86%). The wounds treated with the control sample existed even after 14 days, whereas the wounds treated with DMN@TCH/DFO mostly healed, with a wound healing ratio of 90.53 ± 2.22%. These results suggest that DMN@TCH/DFO exhibited the best wound healing efficacy compared with the other groups, which could be explained by its antibacterial and pro-angiogenic properties.

The histological analysis of wounds is important to assess the extent of wound healing. A histological examination was conducted to evaluate the wound-healing effect using H&E staining on day 14. In DMN@TCH/DFO, mature granulation tissue was formed, developing the basic structures of the epithelium and dermis, and the epidermis further produced basal, spinous, and granular layers (Fig. 4e). However, the control sample was only in the early stages of granulation tissue formation, and the blank DMN was less compact, accompanied by incomplete regeneration of the epidermal and dermal tissue.

Collagen deposition occurs throughout the wound healing process and plays a crucial role in diabetic wound healing and skin remodeling.[37] When granulation tissue is formed, fibroblasts continuously synthesize collagen, and collagen fibers and tissue provide a scaffold for cell migration. Therefore, the amount of collagen deposition is an important indicator of wound repair.[38] Here, Masson staining was used to detect nascent collagen deposition on day 14 after treatment. As shown in Fig. 4f, although new collagen deposition and regenerated tissue were formed in each sample, collagen deposition in DMN@TCH/DFO was more regularly arranged, more evenly distributed, and more mature. These results suggest that DMN@TCH/DFO promotes diabetic wound repair by accelerating fibroblast migration and proliferation, granulation tissue formation, and collagen deposition.

Long-term exposure to high levels of TNF-α adversely affects wound healing.[39] To further confirm the inflammation regulation process of DMN@TCH/DFO, the immunohistochemical staining of TNF-α in the regenerated tissues was performed. As shown in Fig. 5a, the expression of TNF-α in DMN@TCH/DFO was significantly lower than that in the control and blank DMN samples at different points of time. Simultaneously, the inflammatory response to treatment with the control and blank DMN samples tended to increase from day 3 to 7, whereas the inflammatory response with DMN@TCH/DFO was significantly attenuated, with almost no inflammation or infection on day 7. Therefore, DMN@TCH/DFO exhibits anti-infective effects.

In the early stages of skin wound healing, a large number of new capillaries appear in the wound tissue, providing a blood supply for wound healing and bringing nutrients, oxygen, and immune cells. When the skin is damaged, larger

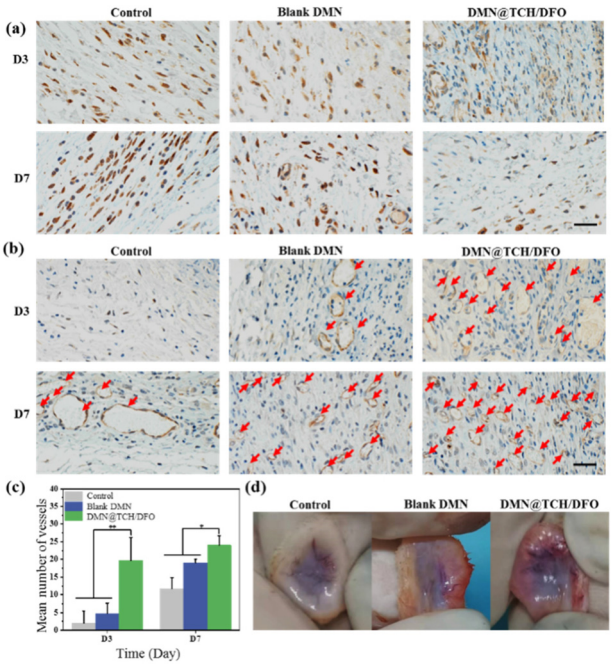

Fig. 5 (a) TNF-α staining of wounds on days 3 and 7 (scale bar: 100 μm); (b) CD31 staining of wounds on days 3 and 7. Red arrows indicate blood vessels (scale bar: 100 μm); (c) mean number of vessels calculated from CD31 stained wound sections (mean ± SD, n = 3),*p < 0.05, **p < 0.01; (d) subcutaneous vascularization of wound tissue on day 7 post-treatment.

blood vessels appear in the wound, allowing the formation of granulation tissue. In the later stages of healing, the blood vessels degenerate to the level of normal tissue. Therefore, the promotion of blood vessel remodeling and maturation is crucial for treatment.[40] Subcutaneous vascularization of the wound tissue was assessed on day 7 post-treatment. To further assess angiogenesis during wound healing, expression of the vascular marker CD31 was detected by immunohistochemical staining. The number of blood vessels was calculated from these images. As shown in Fig. 5b and c, DMN@TCH/DFO displayed the highest CD31 expression, and the number of new blood vessels in the wounds treated with DMN@TCH/DFO was higher than that treated with the blank DMN and control samples on days 3 and 7. As shown in Fig. 5d, fewer subcutaneous blood vessels were observed in the wounds treated with the blank DMN and control samples, indicating poor angiogenesis, but a large number of new blood vessels were formed subcutaneously in the wounds treated with DMN@TCH/DFO. On day 7, the blank DMN was in the early stages of granulation tissue formation; thus, the blood vessels formed were thicker. At this time, the blood vessels in the DMN@TCH/DFO-treated wounds were transformed into dense microvessels. These results confirm that DMN@TCH/DFO stimulates the rapid generation of new blood vessels.

During wound healing, new collagen is mainly derived from fibroblasts and this determines the tensile strength of the skin. The type and amount of collagen change during healing. Collagen III is the first collagen to be synthesized in

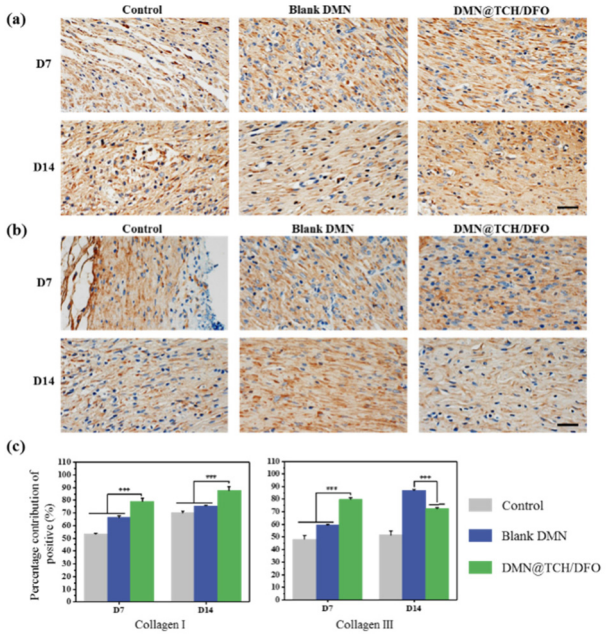

Fig. 6 (a) Collagen I and (b) collagen III immunohistochemical staining of wounds on days 7 and 14 (scale bar: 100 μm); (c) the percentage contribution of positive of collagen I and collagen III (mean ± SD, n = 3), ***$p < 0.001$.

the initial stages of wound healing and is gradually replaced by collagen I as a wound heals.[41] We assessed collagen I/III content by the immunohistochemical staining of the wound tissue. Fig. 6 shows the expression levels of type I and type III collagens. On day 7, wound healing was in the early stages, and DMN@TCH/DFO demonstrated the highest type III collagen expression. On day 14, scar tissue formed at the wound. When compared with the other two samples, the wounds treated with DMN@TCH/DFO showed the highest type I collagen deposition, which was also greater than that of type III collagen. Collagen deposition aids wound healing; therefore, DMN@TCH/DFO can promote wound recovery.

The results showed that the blank DMN also had a certain effect on promoting wound healing, which may be attributed to the good biological activity of the microneedle matrix. HA can promote cell motility and proliferation, and regulate cell adhesion to the extracellular matrix.[22] CS has the function of stimulating the formation of granulation tissue. SF also promotes wound healing by altering the expression of proteins involved in the remodeling and proliferative phases by stimulating NF-κB signaling.[42] Based on this, DMN@TCH/DFO can release TCH to achieve sterilization and DFO to promote angiogenesis at the wound site, thereby reducing inflammation, promoting collagen deposition, and accelerating wound healing.

4. Conclusions

In summary, we developed a novel multifunctional double-layer drug-loaded microneedle, *viz.*, DMN@TCH/DFO, with excellent antibacterial and angiogenic properties for diabetic wound healing. The double-layer microneedle tip was prepared using hyaluronic acid and possessed a fast-dissolving ability. The microneedle substrate was a mixture of chitosan and silk fibroin with swelling capabilities. The double-layer microneedle exhibited a regular morphology, a uniform structure, and an excellent transdermal effect. Antibacterial assays confirmed that the microneedle-loaded TCH in the tip presented significant antibacterial ability against both *E. coli* and *S. aureus* owing to the rapid dissolution of hyaluronic acid and TCH release. The microneedle possessed good biocompatibility and promoted HUVEC tube formation when the substrate of the microneedle was loaded with DFO. In a wound model of diabetic rats, DMN@TCH/DFO significantly accelerated wound healing by improving antibacterial ability, reducing the inflammatory response, promoting angiogenesis, and facilitating collagen deposition. Overall, the multifunctional double-layer drug-loaded microneedle proposed in this study offers a new alternative for diabetic wound repair and may significantly accelerate wound healing.

Author contributions

Shan Gao: conceptualization, investigation, methodology, and writing — original draft. Wanlin Zhang: investigation, methodology, and visualization. Xingxing Zhai: investigation. Xue Zhao: investigation. Jianxin Wang: investigation and supervision. Jie Weng: conceptualization, methodology, supervision, data curation, funding acquisition, and project administration. Xingyu Chen: conceptualization, methodology, supervision, data curation, funding acquisition, project administration, and writing — review and editing. Jianshu Li: investigation and supervision.

Conflicts of interest

There are no conflicts to declare.

Acknowledgements

This work was supported by the National Natural Science Foundation of China (52173140; 52071277), Sichuan Province Science and Technology (2021YJ0192), the R & D Project in Key Areas of Guangdong (No. 2019B 010941002), and the Fundamental Research Funds for the Central Universities (2682020ZT89).

References

1 J. R. Bardill, M. R. Laughter, M. Stager, K. W. Liechty, M. D. Krebs and C. Zgheib, *Acta Biomater.*, 2022, **138**, 73–91.
2 M. V. Vellayappan, S. K. Jaganathan and A. Manikandan, *RSC Adv.*, 2016, **6**, 114859–114878.
3 G. Han and R. Ceilley, *Adv. Ther.*, 2017, **34**, 599–610.

4 A. S. MacLeod, *Cell Host Microbe*, 2019, **25**, 638–640.
5 A. Banu, M. M. Noorul Hassan, J. Rajkumar and S. Srinivasa, *Aust. Med. J.*, 2015, **8**, 280–285.
6 C. Pouget, C. Dunyach-Remy, A. Pantel, S. Schuldiner, A. Sotto and J.-P. Lavigne, *Microorganisms*, 2020, **8**, 1580.
7 U. A. Okonkwo and L. A. DiPietro, *Int. J. Mol. Sci.*, 2017, **18**, 1419.
8 M. Chang and T. T. Nguyen, *Acc. Chem. Res.*, 2021, **54**, 1080–1093.
9 R. E. Jones, D. S. Foster and M. T. Longaker, *J. Am. Med. Assoc.*, 2018, **320**, 1481–1482.
10 E. Everett and N. Mathioudakis, *Ann. N. Y. Acad. Sci.*, 2018, **1411**, 153–165.
11 D. Dayya, O. J. O'Neill, T. B. Huedo-Medina, N. Habib, J. Moore and K. Iyer, *Adv. Wound Care*, 2022, **11**, 12.
12 S. C. Wu and D. G. Armstrong, *Plast. Reconstr. Surg.*, 2006, **117**, 248S–253S.
13 B. A. Lipsky, *Diabetes/Metab. Res. Rev.*, 2016, **32**, 246–253.
14 M. Georgescu, C. M. Chifiriuc, L. Marutescu, I. Gheorghe, V. Lazar, A. Bolocan and S. Bertesteanu, *Curr. Org. Chem.*, 2017, **21**, 53–63.
15 Y. Hao, W. Li, X. Zhou, F. Yang and Z. Qian, *J. Biomed. Nanotechnol.*, 2017, **13**, 1581–1597.
16 X. Yu, J. Zhao and D. Fan, *Chem. Eng. J.*, 2022, **437**, 135475.
17 Y. Su, A. McCarthy, S. L. Wong, R. R. Hollins, G. Wang and J. Xie, *Adv. Healthcare Mater.*, 2021, **10**, 2100135.
18 J. Xu, R. Danehy, H. Cai, Z. Ao, M. Pu, A. Nusawardhana, D. Rowe-Magnus and F. Guo, *ACS Appl. Mater. Interfaces*, 2019, **11**, 14640–14646.
19 I. Woodhouse, S. Nejati, V. Selvamani, H. Jiang, S. Chittiboyina, J. Grant, Z. Mutlu, J. Waimin, N. S. Abutaleb, M. N. Seleem and R. Rahimi, *ACS Appl. Bio Mater.*, 2021, **4**, 5405–5415.
20 J. Chi, L. Sun, L. Cai, L. Fan, C. Shao, L. Shang and Y. Zhao, *Bioact. Mater.*, 2021, **6**, 3507–3514.
21 Y. Sun, J. Liu, H. Wang, S. Li, X. Pan, B. Xu, H. Yang, Q. Wu, W. Li, X. Su, Z. Huang, X. Guo and H. Liu, *Adv. Funct. Mater.*, 2021, **31**, 2100218.
22 X. Zhao, X. Li, P. Zhang, J. Du and Y. Wang, *J. Controlled Release*, 2018, **286**, 201–209.
23 Y.-H. Chiu, M.-C. Chen and S.-W. Wan, *Biomacromolecules*, 2018, **19**, 2278–2285.
24 H. Liu, C. Wang, C. Li, Y. Qin, Z. Wang, F. Yang, Z. Li and J. Wang, *RSC Adv.*, 2018, **8**, 7533–7549.
25 Z. Xu, T. Chen, K.-Q. Zhang, K. Meng and H. Zhao, *Polym. Int.*, 2021, **70**, 1741–1751.
26 M. Zhu, Y. Liu, F. Jiang, J. Cao, S. C. Kundu and S. Lu, *ACS Biomater. Sci. Eng.*, 2020, **6**, 3422–3429.
27 S. Wang, M. Zhu, L. Zhao, D. Kuang, S. C. Kundu and S. Lu, *ACS Biomater. Sci. Eng.*, 2019, **5**, 1887–1894.
28 L.-Y. Long, W. Liu, L. Li, C. Hu, S. He, L. Lu, J. Wang, L. Yang and Y.-B. Wang, *Nanoscale*, 2022, **14**, 1285–1295.
29 T. Ning, F. Yang, D. Chen, Z. Jia, R. Yuan, Z. Du, S. Liu, Y. Yu, X. Dai, X. Niu and Y. Fan, *Adv. Healthcare Mater.*, 2022, **11**, 2102180.
30 M. Winterhalter and M. Ceccarelli, *Eur. J. Pharm. Biopharm.*, 2015, **95**, 63–67.
31 M. Ram, V. Singh, S. Kumawat, D. Kumar, M. C. Lingaraju, T. Uttam Singh, A. Rahal, S. Kumar Tandan and D. Kumar, *Eur. J. Pharmacol.*, 2015, **764**, 9–21.
32 Z. Hou, C. Nie, Z. Si and Y. Ma, *Diabetes Res. Clin. Pract.*, 2013, **101**, 62–71.
33 P. Holden and L. S. Nair, *Tissue Eng., Part B*, 2019, **25**, 461–470.
34 H. Chen, R. Cheng, X. Zhao, Y. Zhang, A. Tam, Y. Yan, H. Shen, Y. S. Zhang, J. Qi, Y. Feng, L. Liu, G. Pan, W. Cui and L. Deng, *NPG Asia Mater.*, 2019, **11**, 3.
35 L. Wu, S. Gao, T. Zhao, K. Tian, T. Zheng, X. Zhang, L. Xiao, Z. Ding, Q. Lu and D. L. Kaplan, *Biomater. Sci.*, 2021, **9**, 3162–3170.
36 H. Chen, L. Guo, J. Wicks, C. Ling, X. Zhao, Y. Yan, J. Qi, W. Cui and L. Deng, *J. Mater. Chem. B*, 2016, **4**, 3770–3781.
37 J. Liu, R. Huang, G. Li, D. L. Kaplan, Z. Zheng and X. Wang, *Biomacromolecules*, 2021, **22**, 546–556.
38 W. Zhao, Y. Li, X. Zhang, R. Zhang, Y. Hu, C. Boyer and F.-J. Xu, *J. Controlled Release*, 2020, **323**, 24–35.
39 R. J. Bodnar, T. Yang, L. H. Rigatti, F. Liu, A. Evdokiou, S. Kathju and L. Satish, *Cytotherapy*, 2018, **20**, 1046–1060.
40 L. A. DiPietro, *J. Leukocyte Biol.*, 2016, **100**, 979–984.
41 S. M.-S. Shomita, R. Sashwati and K. S. Chandan, *Bioengineering*, 2021, **8**, 63.
42 M. Vidya and S. Rajagopal, *Int. J. Polym. Sci.*, 2021, **2021**, 9069924.